Timing PPM-UWB Signals in Ad Hoc Multi-Access

Liuqing Yang, *Member, IEEE*

***Abstract*— To synchronize Ultra-Wideband (UWB) signals with pulse position modulation (PPM), we develop and test timing algorithms in both data-aided and non-data-aided modes based on a novel synchronization criterion that we term Timing with Dirty Templates (TDT). Using symbol-rate integrate-and-dump operations, our TDT-based algorithms for PPM-UWB signals remain operational in practical UWB settings. In addition, our algorithms ensure rapid synchronization by collecting multipath energy. Moreover, for the data-aided mode, we design a simple training pattern which not only expedites the synchronization, but also enables timing in a (possibly ad hoc and asynchronous) multi-user environment. Simulations and comparisons are also performed to corroborate our theoretical analysis.**

***Index Terms*— ultra-wideband, pulse position modulation, timing, synchronization, multipath channel, multi-access**

I. Introduction

UWB radios have attracted increasing interest due to their potential to offer ultra-high user/data capacity with low-complexity, low-power transceivers (see e.g., [4], [9], [13], [16]). However, realization of these potentials heavily hinges upon accurate timing synchronization [8], [11]. As the UWB waveforms are low-power and impulse-like, synchronization is one of the most critical challenges in enabling UWB radios. Additionally, compared to narrowband systems, the difficulty of timing UWB signals is also induced by the (dense) multipath channel that remains unknown at the synchronization stage. Moreover, in UWB systems, pulse position modulation (PPM) is often adopted to reduce transceiver complexity by avoiding pulse negation. However, the difficulty of accurate timing is accentuated in PPM-UWB systems due to the fact that information is conveyed by the shifts of the pulse positions. Such a nonlinear operation is to be contrasted to pulse amplitude modulation (PAM).

In UWB research, synchronization has been intensively studied under various operating environments (see e.g., [1], [2], [5], [6], [7], [14], [17], [18]). Among these works, several remain operational in practical UWB settings and in the presence of multiple users. These include the timing algorithms based on dirty templates (TDT) [14], [17] and the one that capitalizes on a special asymmetric modulation [7]. However, they are all developed for *linearly* modulated PAM-UWB. Since their operations heavily rely on the zero-mean property of PAM, these existing timing algorithms are not applicable to *nonlinearly* modulated PPM-UWB signals.

In this paper, we develop timing algorithms for PPM-UWB signals with direct sequence (DS) and/or time-hopping (TH) spreading. Most existing synchronizers are based on the maximum likelihood principle that requires a "clean template" of the received pulse. However, the latter is not available when the multipath channel is unknown. Our algorithms are developed based on the "dirty templates" as in [14], [17], capitalizing on the novel synchronization criterion of TDT that exploits the unique maximum of the cross correlation of "dirty templates" extracted from the received waveform. As a result, our algorithms rely on symbol-rate samples and are capable of collecting multipath energy without knowledge of the propagation channel. The energy collection in turn expedites the synchronization process. In addition to spectrally efficient non-data-aided (a.k.a. blind) algorithms, we also carefully design training patterns that further reduce the acquisition time. More importantly, we show that these data-aided algorithms remain operational in the presence of multiple interfering users that can be ad hoc and thus asynchronous. Unlike existing algorithms for multi-access PAM-UWB systems in [7], [14], [17], our synchronizers are unique in that they can cope with interfering users transmitting *non-zero mean* PPM signals.

Notation: $\lfloor\cdot\rfloor$ stands for integer floor operation; $\mathrm{E}_s\{\cdot\}$ represents expectation with respect to the random variable s; we will use $\mathrm{var}\{\cdot\}$ to denote variance operation, and $\{A\}_B$ for the modulo operation with base B.

II. Modeling and Preliminaries

In impulse-radio UWB multiple access, every information symbol is transmitted over a time-interval of T_s seconds that consists of N_f frames, each of duration T_f. During each frame, a data modulated ultra short pulse $p(t)$ with duration $T_p \ll T_f$ is transmitted. To ensure low complexity, binary modulations are often adopted. User separation is accomplished with DS and/or TH codes [10], [13]. With PPM modulation, the transmitted waveform is:

$$v^{(u)}(t) = \sqrt{\mathcal{E}_u}\sum_{k=0}^{+\infty} p_T^{(u)}(t - kT_s - s_k^{(u)}\Delta),$$

where $\mathcal{E}_u$ is the u-th user's energy per pulse, Δ is the PPM modulation index, and $p_T^{(u)}(t)$ denotes the *transmitted* symbol waveform

$$p_T^{(u)}(t) := \sum_{n=0}^{N_f-1} c_{ds}^{(u)}(n)\; p(t - nT_f - c_{th}^{(u)}(n)T_c)\;, \qquad (1)$$

which consists of N_f pulses amplitude-modified by the user-specific DS code $c_{ds}^{(u)}(n)$ and/or position-shifted by the TH code $c_{th}^{(u)}(n) = 0, 1, \ldots, N_c$ with $N_c := T_f/T_c$.

The multipath channel is modeled as a tapped-delay line, with $(L_u + 1)$ taps whose amplitudes $\{\alpha_l^{(u)}\}_{l=0}^{L_u}$ and delays $\{\tau_l^{(u)}\}_{l=0}^{L_u}$ satisfy $\tau_l^{(u)} < \tau_{l+1}^{(u)}$, $\forall l$. With the receiver frontend acting as an ideal bandpass filter with ultra-wide bandwidth $B \approx 1/T_p$ centered at ω_0, the aggregate waveform from all

The manuscript was received March 1, 2005; revised October 15, 2005; accepted November 2, 2005. Part of this work was presented at the *Conference on Information Sciences and Systems*, The Johns Hopkins University, Baltimore, March 16-19, 2005.

The author is with the Department of Electrical and Computer Engineering, University of Florida, Gainesville, FL 32611 USA (e-mail: lqyang@ece.ufl.edu).

users at the receive-filter output is:

$$r(t) = \sum_{u=0}^{N_u-1} \sqrt{\mathcal{E}_u} \sum_{l=0}^{L_u} \alpha_l^{(u)} v^{(u)}(t - \tau_l^{(u)}) + \eta(t), \quad (2)$$

where N_u is the total number of active users and $\eta(t)$ is the bandpass filtered zero-mean additive Gaussian noise (AGN) with power spectral density $N_0/2$. Denoting multipath delays $\tau_{l,0}^{(u)} := \tau_l^{(u)} - \tau_0^{(u)}$ relative to the first arrival, the propagation delay $\tau_0^{(u)}$ can be decoupled from the dispersive channel:

$$r(t) = \sum_{u=0}^{N_u-1} \sqrt{\mathcal{E}_u} \sum_{l=0}^{L_u} \alpha_l^{(u)} v^{(u)}(t - \tau_{l,0}^{(u)} - \tau_0^{(u)}) + \eta(t). \quad (3)$$

Notice that the offsets $\tau_0^{(u)}$ in (3) can be different across users, and allow for asynchronous ad hoc multi-access. Let us also introduce the aggregate *received* symbol-long waveform capturing the pulse shaper and the dispersive channel

$$p_R^{(u)}(t) := \sum_{l=0}^{L_u} \alpha_l^{(u)} p_T^{(u)}(t - \tau_{l,0}^{(u)}). \quad (4)$$

Notice that $p_R^{(u)}(t)$ contains the DS and/or TH spreading codes through $p_T^{(u)}(t)$ [c.f. (1)]. To develop our TDT-based algorithms, we assume:

(as) *The nonzero support of waveform $p_R^{(u)}(t)$ is upper bounded by the symbol duration $T_s - \Delta$.*

This assumption implies that inter-symbol interference (ISI) is absent. However, inter-pulse and inter-frame interferences are allowed. In low-duty-cycle UWB systems, (as) can be satisfied by choosing $T_f \geq \tau_{L,0}^{(u)} + T_p + \Delta$ and $c_{th}^{(u)}(N_f - 1) = 0$; whereas in high-rate UWB radios, this condition can be relaxed as long as guard frames are inserted between symbols, much like zero-padding in narrowband systems.

Using (4), the received waveform in (3) becomes:

$$r(t) = \sum_{u=0}^{N_u-1+\infty} \sum_{k=0} \sqrt{\mathcal{E}_u} \cdot p_R^{(u)} \left(t - kT_s - \tau_0^{(u)} - s_k^{(u)} \Delta\right) + \eta(t). \quad (5)$$

With the channel being quasi-static, $\{\alpha_l^{(u)}, \tau_l^{(u)}\}_{l=0}^{L_u}$ remain invariant over one transmission burst, but can change independently across bursts. Timing synchronization amounts to finding the desired user's timing offset $\tau_0^{(u)}$ during each burst.

III. TDT for Point-to-Point PPM-UWB Links

Let us first focus on a point-to-point link and treat multi-access interference as noise. For notational simplicity, we will drop the user index u in this section.

For PAM-UWB systems, the TDT-based timing algorithms developed in [14], [17] rely on the symbol-rate samples obtained by integrating-and-dumping the products of adjacent "dirty templates" [17, Eq. (5)]:

$$x_{\rm PAM}(k;\tau) = \int_0^{T_s} r_{2k+1}(t;\tau) r_{2k}(t;\tau) dt, \quad \forall \tau \in [0, T_s). \quad (6)$$

The symbol-long segments $r_k(t;\tau) := r(t + kT_s + \tau)$, $\forall t \in [0, T_s)$ serve as templates in the correlation in (6). These segments are "dirty" because they are: i) noisy; ii) distorted by the unknown propagation channel; and iii) subject to the unknown offset τ_0. With PAM modulation, the cross-correlation of successive symbol-long noise-free received segments reaches a *unique maximum magnitude* if and only if these segments are scaled replicas of each other, which is achieved only when $\tau = \tau_0$.[1] However, with PPM signaling, it is impossible to have all symbol-long received segments to be scaled versions of each other, even at the correct timing and in the absence of noise.[2] This is due to the *nonlinear* time shifts introduced by the random information symbols.

Although not applicable to PPM-UWB signals in its current form, the TDT-based timing algorithm has many advantages compared to existing alternatives. Among them, the most preeminent is its capability of collecting multipath energy when channel (and possibly the DS/TH spreading code) is still *unknown*, because such information is embedded in the "dirty templates." These motivate us to develop TDT-based synchronizers for PPM-UWB.

The first step is to find the gist of TDT algorithms for PAM signals in practical UWB settings when noise is also present. In this case, Eq. (6) simplifies to [17, Eq. (10)]:

$$x_{\rm PAM}(k;\tau) = s_{2k}[s_{2k-1}\mathcal{E}_A(\tilde{\tau}_0) + s_{2k+1}\mathcal{E}_B(\tilde{\tau}_0)] + \zeta(k;\tau), \quad (7)$$

where $\tilde{\tau}_0 := \{\tau_0 - \tau\}_{T_s}$ with τ_0 and τ being the timing offset and candidate, respectively, and

$$\mathcal{E}_A(\tilde{\tau}_0) := \mathcal{E} \int_{T_s - \tilde{\tau}_0}^{T_s} p_R^2(t) dt, \quad \mathcal{E}_B(\tilde{\tau}_0) := \mathcal{E} \int_0^{T_s - \tilde{\tau}_0} p_R^2(t) dt.$$

Taking the mean-square of (7) gives rise to [17, Eq. (12)]:

$$\mathrm{E}_{s,\xi}\{x_{\rm PAM}^2(k;\tau)\} = \mathcal{E}_R^2 - \mathcal{E}_A(\tilde{\tau}_0)\mathcal{E}_B(\tilde{\tau}_0) + \sigma_\zeta^2, \quad (8)$$

where $\mathcal{E}_R := \mathcal{E}_A(\tilde{\tau}_0) + \mathcal{E}_B(\tilde{\tau}_0) = \mathcal{E} \int_0^{T_s} p_R^2(t) dt$ is the constant energy of the unknown aggregate template at the receiver and σ_ζ^2 is the noise variance. Since both $\mathcal{E}_A(\tilde{\tau}_0)$ and $\mathcal{E}_B(\tilde{\tau}_0)$ are non-negative energies, $\mathcal{E}_A(\tilde{\tau}_0)\mathcal{E}_B(\tilde{\tau}_0)$ exhibits a unique minimum when $\tilde{\tau}_0 = 0$, since $\mathcal{E}_A(\tilde{\tau}_0) = 0$ and $\mathcal{E}_B(\tilde{\tau}_0)$ is maximized when $\tilde{\tau}_0 = 0$; i.e., at the correct timing $\tau = \tau_0$. Hence, the operation of the TDT algorithms for PAM-UWB hinges upon the energy product $\mathcal{E}_A(\tilde{\tau}_0)\mathcal{E}_B(\tilde{\tau}_0)$. However, once again, Eq. (7) does not hold when PPM is deployed, simply because the PPM symbols are embedded in the *time shift* of $p_R(t)$, as opposed to its *amplitude change* when PAM is deployed.

A. Non-Data-Aided TDT for PPM-UWB

Since the samples $x_{\rm PAM}(k;\tau)$ in (6) are not suitable for estimating τ_0 in PPM-UWB, we will next develop distinct processing of the dirty templates $\{r_k(t)\}$ to form the $\mathcal{E}_A(\tilde{\tau}_0)\mathcal{E}_B(\tilde{\tau}_0)$ term, which the TDT algorithms hinge upon. Specifically, we formulate $x(k;\tau)$ as:

$$x(k;\tau) := \int_0^{T_s} r_{2k+1}(t;\tau)\ \tilde{r}_{2k}(t;\tau) dt, \quad \forall \tau \in [0, T_s). \quad (9)$$
$$\tilde{r}_k(t;\tau) := r_k(t + \Delta;\tau) - r_k(t - \Delta;\tau),$$

To see how (9) enables TDT, let us first consider its noise-free part $\chi(k;\tau) = \int_0^{T_s} \rho_{2k+1}(t;\tau)\ \tilde{\rho}_{2k}(t;\tau) dt$, where $\rho_k(t;\tau)$ and

[1] Noise-only gaps among successively received multipath-distorted pulses can give rise to multiple maxima and may induce a time uncertainty that is upper bounded by T_f. However, such a timing uncertainty does not affect maximum energy capture that determines the BER. It can also be easily removed by invoking the TH code $c_{th}^{(u)}(0)$ of the desired user.

[2] Of course, such could be the case if one transmits an all-1 or all-0 sequence with PPM modulation. But such a sequence renders timing synchronization impossible since no symbol transition occurs.

$\tilde{\rho}_k(t;\tau)$ represent the noise-free parts of $r_k(t;\tau)$ and $\tilde{r}_k(t;\tau)$, respectively. By definition, and using the (as), we have

$$\rho_k(t;\tau) = \sqrt{\mathcal{E}} \sum_{m=0}^{1} p_R(t + mT_s - \tilde{\tau}_0 - s_{k-k_{\tau_0}-m}\Delta), \quad (10)$$
$$\tilde{\rho}_k(t;\tau) = \rho_k(t+\Delta;\tau) - \rho_k(t-\Delta;\tau), \quad \forall t, \tau \in [0, T_s) ,$$

where $\tilde{\tau}_0 := \{\tau_0 - \tau\}_{T_s}$ and $k_{\tau_0} := \lfloor (\tau_0 - \tau)/T_s \rfloor \in \{0, -1\}$. Although k_{τ_0} can induce demodulation delay, it does not affect τ_0 estimation. For notational brevity, we will henceforth omit k_{τ_0}. Using (10), we prove in Appendix I that

Lemma 1 *When the PPM modulation index satisfies $\Delta \ll T_f$, the noise-free part of $x(k;\tau)$ in* (9) *simplifies to*

$$\chi(k;\tau) \approx (s_{2k-1} - s_{2k})\mathcal{E}_A(\tilde{\tau}_0) + (s_{2k} - s_{2k+1})\mathcal{E}_B(\tilde{\tau}_0) . \quad (11)$$

Averaging with respect to the random symbols $\{s_k\}$, the mean-square of $\chi(k;\tau)$ is:

$$\mathrm{E}_s\{\chi^2(k;\tau)\} \approx \frac{1}{2}(\mathcal{E}_R^2 - 3\mathcal{E}_A(\tilde{\tau}_0)\mathcal{E}_B(\tilde{\tau}_0)) , \quad (12)$$

which contains the energy product $\mathcal{E}_A(\tilde{\tau}_0)\mathcal{E}_B(\tilde{\tau}_0)$ and is uniquely maximized at $\tilde{\tau}_0 = 0$. Lemma 1 and (12) suggests that τ_0 can be recovered by peak-picking the mean-square of $\chi(k;\tau)$ in the absence of noise. When AGN $\eta(t)$ is also present, Eq. (9) becomes

$$x(k;\tau) = (s_{2k-1} - s_{2k})\mathcal{E}_A(\tilde{\tau}_0) + (s_{2k} - s_{2k+1})\mathcal{E}_B(\tilde{\tau}_0) + \xi(k;\tau)$$
$$\xi(k;\tau) := \xi_1(k;\tau) + \xi_2(k;\tau) + \xi_3(k;\tau), \quad (13)$$

where the three components of the noise term are given by

$$\xi_1(k;\tau) := \int_0^{T_s} \tilde{\rho}_{2k}(t;\tau)\eta_{2k+1}(t;\tau)dt$$
$$\xi_2(k;\tau) := \int_0^{T_s} \rho_{2k+1}(t;\tau)(\eta_{2k}(t+\Delta;\tau) - \eta_{2k}(t-\Delta;\tau))dt$$
$$\xi_3(k;\tau) := \int_0^{T_s} \eta_{2k+1}(t;\tau)(\eta_{2k}(t+\Delta;\tau) - \eta_{2k}(t-\Delta;\tau))dt$$

with $\eta_k(t;\tau) := \eta(t + kT_s + \tau)$, $\forall t \in [0, T_s)$. Considering the variances of these noise terms, we show in Appendix II that

Lemma 2 *The noise term $\xi(k;\tau)$ can be well approximated as white Gaussian noise with zero mean and variance $\sigma_\xi^2 \approx 2\mathcal{E}_R N_0 + BT_s N_0^2$.*

It follows from Lemmas 1 and 2 that the mean-square of the samples in (9) can be found as:

$$\mathrm{E}_{s,\xi}\{x^2(k;\tau)\} = \mathrm{E}_s\{\chi^2(k;\tau)\} + \mathrm{E}_\xi\{\xi^2(k;\tau)\} \approx \frac{1}{2}(\mathcal{E}_R^2 - 3\mathcal{E}_A(\tilde{\tau}_0)\mathcal{E}_B(\tilde{\tau}_0) + 2\sigma_\xi^2) , \quad (14)$$

which, similar to (8) for PAM signals, is uniquely maximized when $\tilde{\tau}_0 = 0$ ($\tau = \tau_0$). Compactly written, the *non-data aided* TDT yields: $\tau_0 = \arg\max_{\tau \in [0, T_s)} \mathrm{E}_{s,\xi}\{x^2(k;\tau)\}$. Replacing the ensemble mean with its sample mean estimator, we have:

Proposition 1 *Under (as), and when $\Delta \ll T_f$, unbiased and mean-square sense (m.s.s.) consistent non-data-aided (blind) TDT for PPM-UWB signals can be accomplished even when DS and/or TH codes are present and the multipath channel is unknown, using "dirty" T_s-long segments of the received waveform as follows:*

$$\hat{\tau}_{0,nda} = \arg \max_{\tau \in [0, T_s)} y_{nda}(K;\tau),$$
$$y_{nda}(K;\tau) := \frac{1}{K}\sum_{k=1}^{K}\left(\int_0^{T_s} r_{2k}(t;\tau)\tilde{r}_{2k-1}(t;\tau)dt\right)^2 . \quad (15)$$

The estimator $\hat{\tau}_{0,nda}$ in (15) can be shown to be m.s.s. consistent by deriving the mean and variance of the *cost function* $y_{nda}(K;\tau)$ (see Appendix III):

$$m_{nda}(K;\tau) := \mathrm{E}\{y_{nda}(K;\tau)\} = \frac{1}{2}(\mathcal{E}_R^2 - 3\mathcal{E}_A(\tilde{\tau}_0)\mathcal{E}_B(\tilde{\tau}_0) + 2\sigma_\xi^2),$$
$$\sigma^2_{y_{nda}}(K;\tau) := \mathrm{var}\{y_{nda}(K;\tau)\} = \frac{2\sigma_\xi^2}{K}(\mathcal{E}_R^2 - 3\mathcal{E}_A\mathcal{E}_B + \sigma_\xi^2) + \frac{1}{4K}(\mathcal{E}_R^2 - 3\mathcal{E}_A\mathcal{E}_B)^2. \quad (16)$$

It is worth emphasizing that the basic idea behind our TDT estimator is that $\mathcal{E}_A(\tilde{\tau}_0)\mathcal{E}_B(\tilde{\tau}_0)$ is minimized when $\tilde{\tau}_0 = 0$. Although terms $\mathcal{E}_R$ and σ_ξ are unknown because $p_R(t)$ is unknown, they remain constant $\forall \tau$ and thus do not affect the peak-picking operation in finding $\hat{\tau}_0$. Additionally, the variance in (16) decays as $1/K$, confirming that $\hat{\tau}_{0,nda}$ in (15) is m.s.s. consistent.

B. Data-Aided TDT for PPM-UWB

The blind algorithm is particularly attractive for its spectral efficiency. However, the number of samples K required for reliable estimation can be reduced markedly if a *data aided* approach is pursued. From (13), we observe that: i) when $\tilde{\tau}_0 \neq 0$, then $x(k;\tau)$ only contributes noise if $s_{2k-1} = s_{2k} = s_{2k+1}$; and ii) when $\tilde{\tau}_0 = 0$, then $x(k;\tau)$ only contributes noise if $s_{2k} = s_{2k+1}$. To avoid these noise-only contributions that do not contain any timing information, the training sequence $\{s_k\}$ should be designed such that no successive symbols are the same. Hence, the training sequence for data-aided TDT is designed to comprise a repeated pattern $(1, 0)$; that is

$$s_k = \{k+1\}_2 . \quad (17)$$

It can be easily verified that this pattern simplifies (13) to

$$x(k;\tau) = \mathcal{E}_B(\tilde{\tau}_0) - \mathcal{E}_A(\tilde{\tau}_0) + \xi(k;\tau) . \quad (18)$$

Correspondingly, its mean square becomes:

$$\mathrm{E}_\xi\{x^2(k;\tau)\} = \mathcal{E}_R^2 - 4\mathcal{E}_A(\tilde{\tau})\mathcal{E}_B(\tilde{\tau}) + \sigma_\xi^2. \quad (19)$$

With the blind approach it is necessary to take expectation with respect to s_k in order to remove the unknown symbol effects; while the data-aided mode, this is not needed. Hence, the sample mean $K^{-1}\sum_{k=1}^{K} x^2(k;\tau)$ converges faster to its expected value in (19). This can be corroborated by the statistics of the cost function, which we denote as $y_{da1}(K;\tau)$ when the training pattern in (17) is used [c.f. (18) and (19)]:

$$m_{da1}(K;\tau) = \mathcal{E}_R^2 - 4\mathcal{E}_A(\tilde{\tau}_0)\mathcal{E}_B(\tilde{\tau}_0) + \sigma_\xi^2,$$
$$\sigma^2_{y_{da1}}(K;\tau) = \frac{2\sigma_\xi^2}{K}[\mathcal{E}_R^2 - 4\mathcal{E}_A(\tilde{\tau}_0)\mathcal{E}_B(\tilde{\tau}_0) + \sigma_\xi^2] . \quad (20)$$

Comparing (20) with (16), we observe that not only a larger coefficient (4 in (20) versus 3 in (16)) is associated with the critical term $\mathcal{E}_A(\tilde{\tau}_0)\mathcal{E}_B(\tilde{\tau}_0)$, but also $y_{da1}(K;\tau)$ can be obtained much more reliably (i.e., with a smaller variance) than $y_{nda}(K;\tau)$. These will be shown to considerably improve the performance in our ensuing analysis and simulations.

A major benefit of the data-aided mode is very rapid acquisition. In principle, only $K = 1$ pair of received symbol-long segments encompassing as few as 4 training symbols $(1, 0, 1, 0)$ is sufficient. More specifically, with $K = 1$, the

single pair of "dirty templates" consisting of $r_1(t;\tau)$ and $r_2(t;\tau)$ yields

$$x(1;\tau) = \mathcal{E}_B(\tilde{\tau}_0) - \mathcal{E}_A(\tilde{\tau}_0) + \xi(1;\tau),$$

whose square is guaranteed to contain the $\mathcal{E}_A(\tilde{\tau}_0)\mathcal{E}_B(\tilde{\tau}_0)$ term that our TDT-based algorithm relies on. Of course, larger K values will help average out the additive noise effects and thus improve the synchronization performance.

So far, we have seen that the estimator we developed for blind timing in Propositions 1 can be applied to the data-aided mode without any modification, while providing improved synchronization speed and accuracy. In fact, with our judiciously designed training pattern, further improvements are possible. Notice that the estimator (15) relies on three major steps: correlation, averaging and squaring. The training sequence in (17) allows us to swap the order of these steps and alleviate the noise effects. Specifically, in the data-aided mode, it follows from (18) that

$$\mathrm{E}^2_\xi\{x(k;\tau)\} = \mathcal{E}^2_R - 4\mathcal{E}_A(\tilde{\tau})\mathcal{E}_B(\tilde{\tau}).$$

In other words, by taking the *squared-mean* instead of *mean-square*, the noise variance term σ^2_ξ in (19) is eliminated. This observation leads us to the following result of a timing algorithm tailored for our carefully designed training sequence

Proposition 2 *Under (as), and when $\Delta \ll T_f$, data-aided TDT for PPM-UWB signals can be accomplished even when DS and/or TH codes are present and the multipath channel is unknown, using*

$$\hat{\tau}_{0,da2} = \arg\max_{\tau\in[0,T_s)} y_{da2}(K;\tau),$$
$$y_{da2}(K;\tau) := \left(\frac{1}{K}\sum_{k=1}^{K}\int_0^{T_s} r_{2k}(t;\tau)\tilde{r}_{2k-1}(t;\tau)dt\right)^2. \quad (21)$$

As with the blind mode, the data-aided mode requires only symbol rate samples. In addition, with the training pattern in (17)*, the data-aided mode enjoys rapid acquisition relying on as few as four training symbols* $(1,0,1,0)$.

The mean and variance of the cost function $y_{da2}(K;\tau)$ can be obtained as:

$$m_{da2}(K;\tau) = \mathcal{E}^2_R - 4\mathcal{E}_A(\tilde{\tau}_0)\mathcal{E}_B(\tilde{\tau}_0) + \frac{\sigma^2_\xi}{K},$$
$$\sigma^2_{y_{da2}}(K;\tau) = \frac{2\sigma^2_\xi}{K}\left(\mathcal{E}^2_R - 4\mathcal{E}_A(\tilde{\tau}_0)\mathcal{E}_B(\tilde{\tau}_0) + \frac{\sigma^2_\xi}{K}\right). \quad (22)$$

Though (22) bears the same form as (20), they are different in two senses: i) $y_{da2}(K;\tau)$ asymptotically converges to $[\mathcal{E}^2_R - 4\mathcal{E}_A(\tilde{\tau}_0)\mathcal{E}_B(\tilde{\tau}_0)]$ while $y_{da1}(K;\tau)$ does not; and ii) the variance of $y_{da2}(K;\tau)$ is further reduced by $2(K-1)\sigma^4_\xi/K^2$ since the σ^4_ξ term decays as $1/K^2$, thanks to the averaging prior to squaring. These differences can further improve the accuracy of $\hat{\tau}_0$, as we show in the next section.

C. Performance Bounds and Comparisons

Here we compare their performance in a coarse timing (acquisition) setup, where the N_i candidate offsets are $\tau = nT_i$ with integer $n \in [0, N_i - 1]$ and minimum spacing $T_i := T_s/N_i$. Instead of estimating the true τ_0, coarse timing aims at finding n^* such that $|n^*T_i - \tau_0| < T_i$; that is, *detecting* n^* such that $n^* = \arg\max_n\{m(K;nT_i)\}$. Accordingly, the detector unifying Propositions 1 and 2 is: $\widehat{n^*} = \arg\max_n y(K;nT_i)$, and the probability of detection is given by:

$$P_d(n^*) = \Pr\left\{\widehat{n^*} = n^*\right\} = \Pr\left\{y(K;n^*T_i) = \max_n\ y(K;nT_i)\right\}. \quad (23)$$

At any given SNR and regardless of $p_R(t)$ and K, $P_d(n^*)$ depends on n^*, because the noise terms in $y(K;nT_i)$ come from overlapping observation windows and are correlated across n. As in [17], we assume independence among these noise terms for analytical tractability. Under this assumption, our analytical results are rather pessimistic and serve as lower bounds on the true probabilities of detection. Denoting the pdf of $y(K;nT_i)$ as $f_{K,n}(y)$, the probability of detection is $P_d = \int_{-\infty}^{+\infty} f_{K,n^*}(y_0)\prod_{n\neq n^*}\left(\int_{-\infty}^{y_0} f_{K,n}(y_1)dy_1\right)dy_0$, which involves N_i-fold integration and is cumbersome to evaluate, especially for large N_i values. Hence, a tight lower bound with a simple form is desirable. Instead of the union bound that is very loose and can at times be negative at low SNR, we resort to a universally tighter bound, which we derived in [17]:

$$\underline{P}_d = \prod_{n\neq n^*} Q\left(\frac{m(K;n^*T_i) - m(K;nT_i)}{\sqrt{\sigma^2_y(K;n^*T_i) + \sigma^2_y(K;nT_i)}}\right), \quad (24)$$

where $Q(\cdot)$ is the complementary cdf of a standard Gaussian distribution with zero mean and unit variance. Using (16), (20) and (22), and for any given n, n^* and $K > 1$, we have

$$\begin{aligned} &m_{nda}(K;n^*T_i) - m_{nda}(K;nT_i) \\ <&m_{da1}(K;n^*T_i) - m_{da1}(K;nT_i) \\ =&m_{da2}(K;n^*T_i) - m_{da2}(K;nT_i), \\ \text{and}\quad &\sigma^2_{y_{nda}}(K;n^*T_i) + \sigma^2_{y_{nda}}(K;nT_i) \\ >&\sigma^2_{y_{da1}}(K;n^*T_i) + \sigma^2_{y_{da1}}(K;nT_i) \\ >&\sigma^2_{y_{da2}}(K;n^*T_i) + \sigma^2_{y_{da2}}(K;nT_i) \end{aligned} \quad (25)$$

for the estimators corresponding to Propositions 1 and 2, with and without the training sequence. Eqs. (24) and (25) reveal that: $\underline{P}_{d,nda} < \underline{P}_{d,da1} < \underline{P}_{d,da2}$, $\forall K > 1$. As expected, data-aided TDT outperforms blind TDT even with the same estimator in Proposition 1. In addition, the $\hat{\tau}_0$ estimator specifically tailored for the training sequence can further improve the performance, even with the same training pattern in (17).

Although we only examined the coarse timing performance here, it is worth mentioning that the $\hat{\tau}_0$ estimators in Propositions 1 and 2 allow for timing acquisition at any desirable resolution constrained only by the affordable complexity: i) coarse timing with low complexity, e.g., by picking the maximum over N_f candidate offsets $\tau = nT_f$, where integer $n \in [0, N_f)$; ii) fine timing with higher complexity at the chip resolution with $\tau = iT_c$, $i \in [0, N_c)$; and iii) adaptive timing estimation (tracking) with voltage-controlled clock (VCC) circuits. It is also worth mentioning that, though our timing algorithms here are derived for fast TH or DS spreading codes with single-symbol period, the data-aided TDT algorithm can be easily generalized to account for slow TH and DS codes with multi-symbol period, by alternately transmitting 1's and 0's every other TH/DS period.

Summarizing, in a point-to-point link, we derived two $\hat{\tau}_0$ estimators in Propositions 1 and 2. The former applies to both blind and data-aided modes, while the latter relies on our carefully designed training pattern in (17). This training pattern, even with the general estimator in (15), enables faster synchronization with higher accuracy. Tailored for this pattern, the estimator (21) improves performance using the same samples taken at symbol-rate. More importantly, we will prove in Section IV that the estimator (21) remains operational even when multiple (asynchronous) ad hoc users are present.

IV. TDT for Multi-User PPM-UWB Links

Consider now a PPM-UWB system with multiple users that can be ad hoc and asynchronous. The desired user (say user 0) is transmitting the training pattern. The received signal is now embedded in the aggregate of other asynchronous users communicating information-bearing i.i.d. PPM symbols. Eq. (9) then becomes:

$$x(k;\tau)=\sum_{u=0}^{N_u-1}x_u(k;\tau)=\sum_{u=0}^{N_u-1}\left[s_{2k-1}^{(u)}-s_{2k}^{(u)}\right]\mathcal{E}_{u,A}(\tilde{\tau}_0^{(u)}) \quad (26)$$
$$+\left[s_{2k}^{(u)}-s_{2k+1}^{(u)}\right]\mathcal{E}_{u,B}(\tilde{\tau}_0^{(u)})+\xi(k;\tau),$$

where $\tilde{\tau}_0^{(u)}:=\{\tau_0^{(u)}-\tau\}_{T_s}$, $\mathcal{E}_{u,A}(\tilde{\tau}):=\mathcal{E}_u\int_{T_s-\tilde{\tau}}^{T_s}|p_R^{(u)}(t)|^2dt$ and $\mathcal{E}_{u,B}(\tilde{\tau}):=\mathcal{E}_u\int_0^{T_s-\tilde{\tau}}|p_R^{(u)}(t)|^2dt$ are as defined before, but with symbols, channels and offsets being user-dependent. As we argued in Section III, the noise-free part of the desired user's samples of the dirty-template correlator obey [c.f. (18)]:

$$\chi_0(k;\tau)=\mathcal{E}_{0,B}(\tilde{\tau}_0^{(0)})-\mathcal{E}_{0,A}(\tilde{\tau}_0^{(0)}).$$

Substituting into (26), we obtain:

$$x(k;\tau)=\chi_0(k;\tau)+\sum_{u\neq 0}\left[s_{2k-1}^{(u)}-s_{2k}^{(u)}\right]\mathcal{E}_{u,A}(\tilde{\tau}_0^{(u)})$$
$$+\left[s_{2k}^{(u)}-s_{2k+1}^{(u)}\right]\mathcal{E}_{u,B}(\tilde{\tau}_0^{(u)})+\xi(k;\tau).$$

Now averaging (without squaring), we obtain $\mathrm{E}_{s,\xi}\{x(k;\tau)\}=\chi_0(k;\tau)$ simply because $\mathrm{E}_{s,\xi}\{\chi_u(k;\tau)\}=0$. This observation suggests that the single-user TDT estimator we summarized in Proposition 2 is operational even in a multi-user environment:

Proposition 3 *Under (as) and with the desired user transmitting the training pattern in* (17) *and other users transmitting equi-probable i.i.d. information symbols, m.s.s. consistent data-aided TDT can be accomplished with as few as four training symbols using* (21)*. The multiple active users can be synchronous or asynchronous, and no knowledge of these users' channels or timing information is required.*

The algorithm as described in Proposition 3 requires that a receiver can "hear" only a single transmitter's synchronization pattern, regardless of the presence of multiple non-zero-mean interfering PPM signals from other communicating nodes. Such is the case when the ad hoc network has star or clustered topologies. Within each cluster, nodes can take turns to synchronize their neighbors.

At the synchronization stage, the dense multipath channel is typically unknown. Hence, a noise-free and offset-free "clean" template of the distorted waveform is not available.

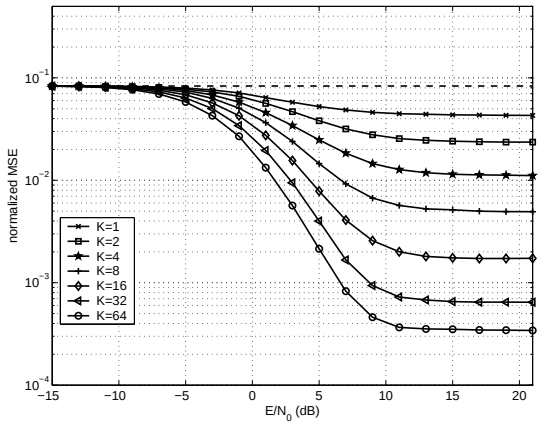

Fig. 1. Normalized MSE of non-data-aided (blind) TDT synchronizer in Proposition 1 with various K values, in a single-user PPM-UWB link.

This renders conventional approaches including the maximum-likelihood timing offset estimator unapplicable. Hence, our TDT-based timing algorithms here are well motivated for such scenarios. But even in AWGN channels where the clean template $p(t)$ is readily available, our algorithms still have clear advantages over conventional ones. In this case, symbol-level (coarse) synchronization is impossible with the conventional synchronizers using the $p(t)$ template, because the frame-by-frame sliding correlation will mostly capture only noise from the received waveform consisting of episodic signals. Therefore, the conventional approaches necessitate performing correlations at all T_p-long intervals throughout a symbol duration of T_s, which translates to searching for the maximum over N_fN_c lags. On the other hand, our algorithms rely on the correlation between two dirty templates subject to the same frame-level shift, which can capture the signal energy even in the coarse timing stage. Hence, synchronization can be achieved in two steps: symbol-level with N_f lags (one per frame) followed by frame-level (fine) synchronization with N_c lags (one per T_p). With typically large N_f and N_c values in low-duty-cycle UWB, the complexity reduction (e.g., 94% with $N_f=32$ and $N_c=35$) can be very significant.

V. Simulations

In this section, simulations are carried out to test the performance of our TDT-based algorithms for PPM-UWB signals. The UWB pulse is the second derivative of the Gaussian function with unit energy and duration $T_p\approx 1$ns. The multipath channels are generated using the channel model in [3] with real channel taps and parameters $(1/\Lambda,1/\lambda,\Gamma,\gamma)=(43,0.4,7.1,4.3)$ns. Other system parameters are $\Delta=1$ns, $T_f=35$ns and $N_f=32$. The timing offset τ_0 is randomly generated from a uniform distribution over $[0,T_s)$. We use a random TH code uniformly distributed over $[0,N_c-1]$, with $N_c=35$, and $T_c=2$ns. In all simulations, only frame-level coarse timing is performed.

The timing estimate mean-square error (MSE) normalized with respect to T_s^2 is plotted versus $\mathcal{E}/N_0$ in Figs. 1 and 2 for the algorithm summarized in Proposition 1, with and without training symbols. It is evident that the data-aided algorithm has better estimation performance than the blind one, at the price of reduced bandwidth efficiency. At medium

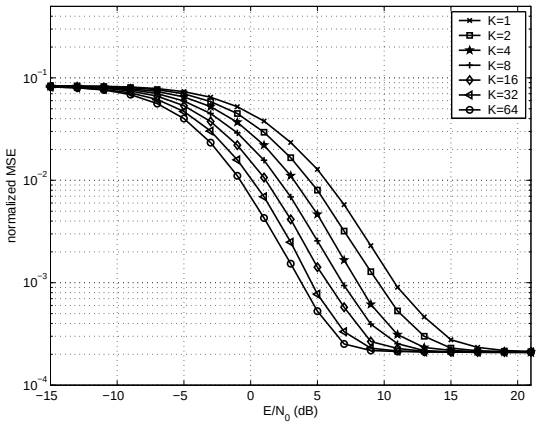

Fig. 2. Normalized MSE of the TDT synchronizer in Proposition 1 with our training sequence (17), in a single-user PPM-UWB link.

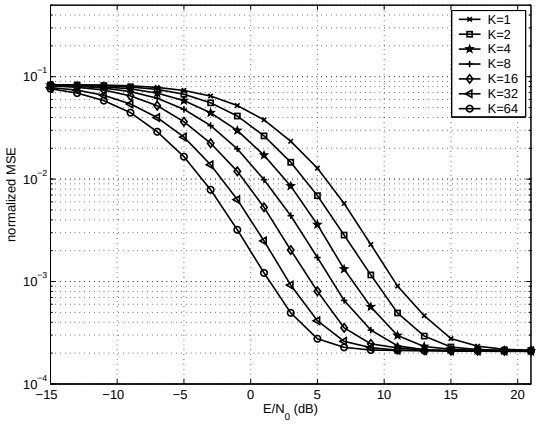

Fig. 3. Normalized MSE of the data-aided TDT synchronizer in Proposition 2 with our training sequence (17), in a single-user PPM-UWB link.

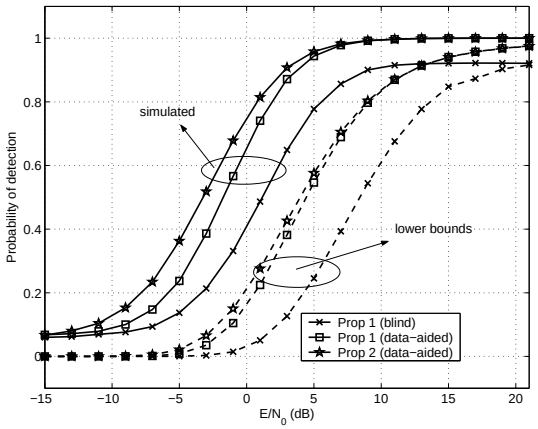

Fig. 4. Probability of detection and its lower bound versus SNR with $K = 16$, in a single-user PPM-UWB link.

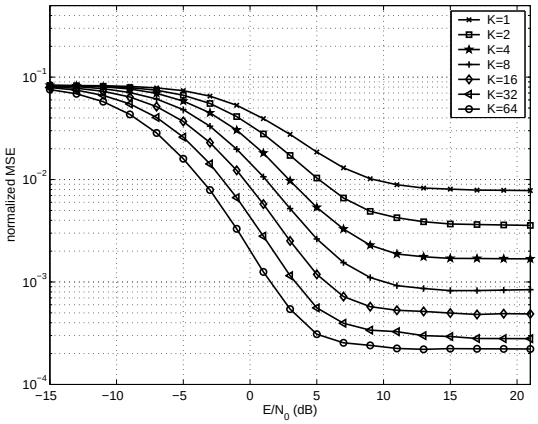

Fig. 5. Normalized MSE of the data-aided TDT synchronizer with our training sequence (17), in a multi-user PPM-UWB environment.

SNR, all curves reach an error floor, since only coarse timing with T_f resolution is performed. This error floor can be mitigated by fine timing (tracking). In the blind mode, error floors at different levels are observed when K varies. This is because the blind mode relies on the averaging with respect to information symbols; and larger K values induces better averaging.

The TDT-based synchronizer in Proposition 2 is specifically tailored for our carefully designed training pattern. Its MSE performance is shown in Fig. 3. The curve corresponding to $K = 1$ pair of dirty templates is identical to that in Fig. 2. But when $K > 1$, the estimator (21) consistently outperforms (15) with the same training pattern in (17), and the gap between the two increases as K increases.

Fig. 4 depicts the simulated probabilities of detection and their analytical lower bounds in (24) for the TDT synchronizers in Propositions 1 and 2, with $K = 16$ pairs of dirty templates. As mentioned before, these bounds are relatively pessimistic compared to the simulated performance, but can be used to predict the relative performance of these timing algorithms.

In Fig. 5, the normalized MSE corresponding to (21) in the presence of two interfering users is shown. The two interfering users both transmit non-zero-mean PPM signals, and the desired user uses the training pattern in (17). All users are mutually asynchronous. The SNR of the two interferers is 6dB and 10dB weaker than the desired user's signal, respectively. Due to the multi-access interference, the normalized synchronization MSE exhibits K-dependent error floors.

VI. Conclusions

In this paper, we developed low-complexity timing algorithms for nonlinear PPM-UWB signals based on the concept of dirty templates. Our algorithms are derived in both data-aided and non-data-aided (blind) modes. Their performance is tested and compared by analysis and simulations. Both algorithms remain operational in general UWB settings without imposing impractical assumptions, and ensure rapid timing by collecting the rich multipath energy provided by UWB channels. In the blind mode, timing information is acquired with symbol-rate samples and without sacrificing bandwidth efficiency. In the data-aided mode, we carefully designed a simple training pattern. Deployment of this pattern renders synchronization more rapid and accurate, and enables timing a desired user in a multi-access environment with ad hoc (and possibly asynchronous) users.

Appendix I: Proof of Lemma 1

Substituting (10) into (11), we obtain

$$\begin{aligned}\chi(k;\tau) = &\mathcal{E}\int_{T_s-\tilde{\tau}_0}^{T_s} p_R(t-s_{2k}\Delta)\tilde{p}_R(t-s_{2k-1}\Delta)dt \\ &+\mathcal{E}\int_{0}^{T_s-\tilde{\tau}_0} p_R(t-s_{2k+1}\Delta)\tilde{p}_R(t-s_{2k}\Delta)dt,\end{aligned} \tag{27}$$

because $p_R(t)$ and $p_R(t+T_s)$ are non-overlapping. If two symbols take the same value $s_k = s_l$, and when $\Delta \ll T_f$, we have

$$\int p_R(t-s_k\Delta)\tilde{p}_R(t-s_l\Delta)dt = \int p_R(t-s_k\Delta)p_R(t-s_k\Delta+\Delta)dt - \int p_R(t-s_k\Delta)p_R(t-s_k\Delta-\Delta) \approx 0. \quad (28)$$

If the binary PPM symbols $s_k \neq s_l$, then $s_k = s_l \pm 1$ and

$$\tilde{p}_R(t-s_l\Delta) := p_R(t-s_l\Delta+\Delta) - p_R(t-s_l\Delta-\Delta) = (s_l-s_k)[p_R(t-s_k\Delta) - p_R(t-s_k\Delta-2(s_l-s_k)\Delta)] .$$

Accordingly, $\int p_R(t-s_k\Delta)\tilde{p}_R(t-s_l\Delta)dt = (s_l-s_k)[\int p_R^2(t-s_k\Delta)dt - \int p_R(t-s_k\Delta)p_R(t-s_k\Delta-2(s_l-s_k)\Delta)dt]$, where the second integral is negligible compared to the first term. Summarizing, we have:

$$\int p_R(t-s_k\Delta)\tilde{p}_R(t-s_l\Delta)dt \approx (s_l-s_k)\int p_R^2(t-s_k\Delta)dt \ , \quad (29)$$

which subsumes (28) as a special case when $s_l = s_k$. Substituting (29) into (27) concludes the proof of Lemma 1.

APPENDIX II: PROOF OF LEMMA 2

For notational brevity, we will temporarily drop the notion of τ in $\xi(k;\tau)$. Along the lines of [15, Appendix I], it can be shown that the noise term $\xi(k)$ has zero mean because all its components $\xi_1(k)$, $\xi_2(k)$ and $\xi_3(k)$ are zero-mean and mutually independent Gaussian random variables. Hence, its variance is given by $\sigma_\xi^2 = \sigma_{\xi_1}^2 + \sigma_{\xi_2}^2 + \sigma_{\xi_3}^2$. Starting with $\xi_1(k)$,

$$\sigma_{\xi_1}^2 = N_0 \cdot \mathrm{E}_s \left\{ \int_0^{T_s} \rho_{2k+1}^2(t)dt - \int_0^{T_s} \rho_{2k+1}(t)\rho_{2k+1}(t-2\Delta)dt \right\}.$$

Since the second term is negligible compared to the first term, we deduce that the variance of $\xi_1(k)$ is $\sigma_{\xi_1}^2 \approx \mathcal{E}_R N_0$. The variance of the noise component $\xi_2(k)$, by definition, is

$$\sigma_{\xi_2}^2 = \mathrm{E}_{s,\eta} \left\{ \int_0^{T_s} \int_0^{T_s} \tilde{\rho}_{2k}(t)\tilde{\rho}_{2k}(\lambda)\eta_{2k+1}(t)\eta_{2k+1}(\lambda)dtd\lambda \right\},$$

where $\tilde{\rho}_k(t)$ is defined in (10). Using the fact that $\Delta \ll T_s$, we have $\sigma_{\xi_2}^2 \approx \mathcal{E}_R N_0$.

The noise component $\xi_3(k)$ contain the "double-noise" term, whose variance is given by

$$\sigma_{\xi_3}^2 = 2\int_0^{T_s}\int_0^{T_s} \mathrm{E}_\eta\{\eta_{2k+1}(t)\eta_{2k+1}(\lambda)\eta_{2k}(t)\eta_{2k}(\lambda)\}dtd\lambda - 2\int_0^{T_s}\int_0^{T_s} \mathrm{E}_\eta\{\eta_{2k+1}(t)\eta_{2k+1}(\lambda)\eta_{2k}(t-\Delta)\eta_{2k}(\lambda+\Delta)\}dtd\lambda,$$

with the PPM modulation index $\Delta \ll T_s$. It then follows from [15, (42,43)] that $\mathrm{E}_\eta\{\xi_3^2(k)\} \approx N_0^2 B T_s$.

APPENDIX III: PROOF OF EQ. (16)

The expected value of $y_{nda}(K;\tau)$ in (15) can be easily obtained from (19). To obtain its variance, first notice that, depending on k and l values, and with binary PPM, $\mathrm{E}\left\{x^2(k;\tau)x^2(l;\tau)\right\}$ can be computed by considering two cases:

$$\begin{cases} \frac{1}{2}(\mathcal{E}_R^2 - 3\mathcal{E}_A\mathcal{E}_B + 2\sigma_\xi^2)^2 + \sigma_\xi^2(\mathcal{E}_R^2 - 3\mathcal{E}_A\mathcal{E}_B + \sigma_\xi^2), & \text{if } k = l, \\ \frac{1}{4}(\mathcal{E}_R^2 - 3\mathcal{E}_A\mathcal{E}_B + 2\sigma_\xi^2)^2, & \text{else.} \end{cases}$$

Adding them up with appropriate weights, we have:

$$\sigma_{y_{nda}}^2(K;\tau) = \frac{2\sigma_\xi^2}{K}(\mathcal{E}_R^2 - 3\mathcal{E}_A\mathcal{E}_B + \sigma_\xi^2) + \frac{1}{4K}(\mathcal{E}_R^2 - 3\mathcal{E}_A\mathcal{E}_B)^2.$$

REFERENCES

[1] S. Aedudodla, S. Vijayakumaran, and T. F. Wong, "Ultra-wideband signal acquisition with hybrid *ds-th* spreading," *IEEE Trans. on Wireless Communications*, submitted June 2004; revised Jan. 2005.

[2] R. Fleming, C. Kushner, G. Roberts, and U. Nandiwada, "Rapid acquisition for Ultra-Wideband localizers," in *Proc. of Conf. on Ultra-Wideband Systems and Technologies*, Baltimore, MD, May 20-23, 2002, pp. 245–250.

[3] J. R. Foerster, *Channel Modeling Sub-committee Report Final*, IEEE P802.15-02/368r5-SG3a, IEEE P802.15 Working Group for WPAN, November 2002.

[4] J. R. Foerster, E. Green, S. Somayazulu, and D. Leeper, "Ultra-Wideband technology for short or medium range wireless communications," in *Intel Technology Journal Q2*, 2001. [Online]. Available: http://developer.intel.com/technology/itj

[5] E. A. Homier and R. A. Scholtz, "Rapid acquisition of Ultra-Wideband signals in the dense multipath channel," in *Proc. of Conf. on Ultra-Wideband Systems and Technologies*, Baltimore, MD, May 20-23, 2002, pp. 105–110.

[6] J. Y. Lee and R. A. Scholtz, "Ranging in a dense multipath environment using an UWB radio link," *IEEE Journal on Selected Areas in Communications*, vol. 20, no. 9, pp. 1677–1683, December 2002.

[7] X. Luo and G. B. Giannakis, "Low-complexity blind synchronization and demodulation for (ultra-) wideband multi-user ad hoc access," *IEEE Trans. on Wireless Communications*, 2005 (to appear).

[8] D. Porrat and D. Tse, "Bandwidth scaling in Ultra Wideband communications," in *Proc. of 41st Allerton Conf.*, Univ. of Illinois at U-C, Monticello, IL, October 1-3, 2003.

[9] R. C. Qiu, H. Liu, and X. Shen, "Ultra-wideband for multiple access communications," *IEEE Communications Magazine*, vol. 43, no. 2, pp. 80–87, February 2005.

[10] B. M. Sadler and A. Swami, "On the performance of UWB and DS-spread spectrum communication systems," in *Proc. of Conf. on Ultra-Wideband Systems and Technologies*, Baltimore, MD, May 20-23, 2002, pp. 289–292.

[11] Z. Tian and G. B. Giannakis, "BER sensitivity to mis-timing in ultra-wideband communications, part i: Non-random channels," *IEEE Trans. on Signal Processing*, vol. 53, no. 4, pp. 1550–1560, April 2005.

[12] ——, "Data-aided ML timing acquisition in Ultra-Wideband radios," in *Proc. of Conf. on Ultra-Wideband Systems and Technologies*, Reston, VA, November 16-19, 2003, pp. 142–146.

[13] M. Z. Win and R. A. Scholtz, "Ultra wide bandwidth time-hopping spread-spectrum impulse radio for wireless multiple access communications," *IEEE Trans. on Communications*, vol. 48, no. 4, pp. 679–691, April 2000.

[14] L. Yang and G. B. Giannakis, "Low-complexity training for rapid timing acquisition in Ultra-Wideband communications," in *Proc. of Global Telecommunications Conf.*, San Francisco, CA, December 1-5, 2003, pp. 769–773.

[15] ——, "Optimal pilot waveform assisted modulation for Ultra-Wideband communications," *IEEE Trans. on Wireless Communications*, vol. 3, no. 4, pp. 1236–1249, July 2004.

[16] ——, "Ultra-wideband communications: An idea whose time has come," *IEEE Signal Processing Magazine*, vol. 21, no. 6, pp. 26–54, November 2004.

[17] ——, "Timing Ultra-Wideband signals with dirty templates," *IEEE Trans. on Communications*, 2005 (to appear).

[18] L. Yang, Z. Tian, and G. B. Giannakis, "Non-data aided timing acquisition of Ultra-Wideband transmissions using cyclostationarity," in *Proc. of Intl. Conf. on Acoustics, Speech, and Signal Processing,*, Hong Kong, China, April 6-10, 2003, pp. 121–124.

PLACE PHOTO HERE

Liuqing Yang (M'04) received her B.S. degree in Electrical Engineering from Huazhong University of Science and Technology, Wuhan, China, in 1994, and the M.Sc. degree in Electrical and Computer Engineering from the University of Minnesota, in 2002. She is currently a Ph.D. candidate with the Department of Electrical and Computer Engineering, at the University of Minnesota. Her research interests include communications, signal processing and networking. Currently, she has a particular interest in Ultra-Wideband (UWB) communications. Her research encompasses synchronization, channel estimation, equalization, multiple access, space-time coding, and multicarrier systems.